The Dnipro-Buh plume: a tale of high-volume freshwater discharge in a non-tidal sea

Alexander E. Yankovsky[a,*] and Yuriy P. Ilyin[b]

[a] School of the Earth, Ocean and Environment, University of South Carolina, Columbia, SC, 29208, USA

[b] Ukrainian Hydrometeorological Institute, National Academy of Science, Kyiv, 03038, Ukraine

[*] Corresponding author. *E-mail address*: ayankovsky@geol.sc.edu

Highlights:

- The Dnipro-Buh plume rapidly widens with distance from the mouth
- The geostrophic transport of freshwater is a small fraction of the riverine discharge
- Significant upstream penetration of buoyant water occurs without persistent upwelling winds

Abstract

The Dnipro River has the second-largest annually-averaged discharge among European rivers and together with the Pivdennyi Buh River runs off on the Black Sea northwestern shelf, forming the Dnipro-Buh coastal buoyant plume. This study presents shipboard observations of the Dnipro-Buh plume in May of 1992 and 1994, when the freshwater discharge was lower and higher, respectively, than its climatological value for May, while the wind forcing was light and variable. In-situ data are complemented with satellite images obtained under similar forcing conditions at later times. Weak mixing in the Dnipro-Buh estuary leads to the formation of a thin, 1.5-3 m deep surface-advected plume. The estuarine outflow runs off parallel with the coastline, but with downstream distance it rapidly expands offshore over multiple baroclinic Rossby radii. On synoptic to monthly time scales, the Dnipro-Buh plume spreads in bimodal fashion, both upstream and downstream from the estuarine mouth. The downstream geostrophic transport of freshwater in the plume is a small fraction of the freshwater discharge feeding the plume. Also, as salinity anomaly decreases offshore, the freshwater content remains near-constant or even increases. This implies that the freshwater spreading is sustained by cross-frontal "diffusion" to a greater extent than through the advection by geostrophic circulation associated with the plume. Meso- and submesoscale instabilities are likely to play a major role in mixing and offshore spreading of the Dnipro-Buh plume.

Keywords: Black Sea, Dnipro River, freshwater runoff, geostrophic current, wind forcing, mixing.

1. Introduction

The Dnipro (also Dnieper) River has the second-largest freshwater discharge in Europe with the annual average of 1329 m^3s^{-1} (standard deviation of 348 m^3s^{-1}) during 1960-2010, and runs off in the Black Sea (Fig. 1), a semi-enclosed non-tidal sea whose general circulation is strongly affected by the buoyancy forcing (Oguz et al., 1995). The Dnipro River freshwater outflow enters the northwestern shelf (NWS) of the Black Sea through the Dnipro-Buh estuary, which also receives the Pivdennyi Buh (P. Buh, also Southern Bug) River discharge annually averaged at 96 m^3s^{-1} (with a standard deviation of 28 m^3s^{-1}, the same period as for the Dnipro River). Since the Black Sea is a non-tidal basin, the combined Dnipro-Buh outflow undergoes very little mixing in the estuary and reaches its mouth with near-surface salinity of 3-4 psu in April-May, when the discharge is highest through the annual cycle (Ilyin, 2023). Surprisingly little is known about the formation and dynamics of the Dnipro-Buh plume.

The Dnipro-Buh plume resides in the northernmost part of NWS: a shallow (10-20 m depth), semi-enclosed area demarcated by approximately 46°N from the south and separated from the shelfbreak by ~200 km. General characteristics of the study area can be found in the Oceanographic Atlas of the Black Sea and the Sea of Azov (hereinafter, referred to as Atlas). During late April-early June, low-pressure atmospheric systems form over the Black Sea such that prevailing winds over the study area are northeasterly to northerly with velocities less than 5 m s^{-1}. Over this time period, circulation on NWS is cyclonic, currents propagate with the coast on their right, same as a Kelvin wave propagation (hereinafter, referred to as downstream). According to Atlas, average circulation in the study area is predominantly wind driven, and time-averaged surface currents in May don't exceed 0.2 m s^{-1} north of 45.5°N. General circulation of the Black Sea, the Rim Current and its eddies, is confined by the shelfbreak in a deep basin, and has little to no effect on the dynamics in the study area. Even though both the buoyancy and wind forcing support a downstream transport in the study area during late spring, there is significant freshening to the southeast (upstream) from the Dnipro-Buh estuary mouth (Atlas), with the surface monthly-averaged (May) 14-psu isohaline intercepting the coastline to the south of the Tendra Spit tip.

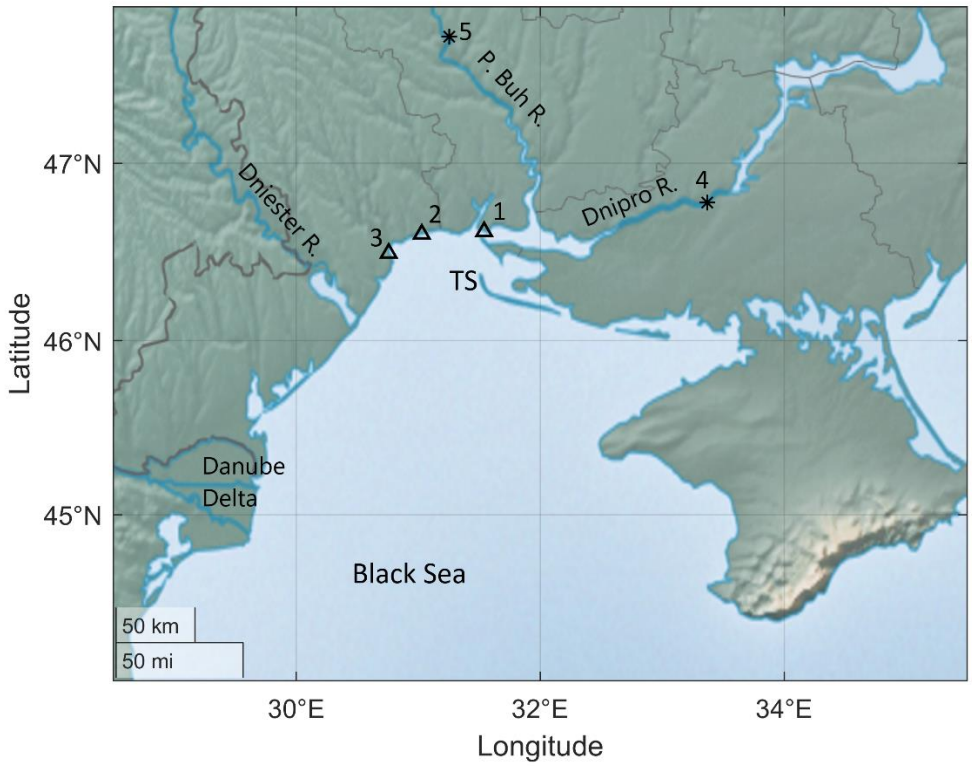

Figure 1. The northwestern Black Sea. Triangles and asterisks are hydrometeorological and streamflow gauge stations, respectively: 1 – Ochakiv, 2 – Yuzhniy, 3 – Odesa, 4 – Kakhovka, 5 – Alexandrovka; TS = Tendra Spit.

Ilyin (2023) assessed climatological characteristics of the Dnipro-Buh estuary including various hydrodynamical parameters of the buoyant outflow on the shelf. In general, estuarine circulation implies an exchange flow through the estuarine mouth, which is driven by estuarine mixing, typically of the tidal origin (e.g., Geyer and MacCready, 2014). The volumetric transport of both branches, the buoyant outflow and the compensating inflow of the shelf water, significantly exceeds the freshwater discharge and depends on the extent of estuarine mixing (MacCready et al., 2018; Burchard et al., 2019). However, this is not the case for the Dnipro-Buh

estuarine outflow due to its low salinity. Using the well-known Knudsen relation, Ilyin (2023) estimated that the outflow volumetric transport exceeds the Dnipro-Buh freshwater discharge by only 20-25% in April-June. Also, the baroclinic Rossby radius of the outflow exceeds the width of the mouth (which is 3.7 km) rendering a Kelvin number (Garvine, 1995) Ke < 1. For Ke < 1, the momentum advection becomes important and the buoyant outflow tends to widen past the mouth. Estuarine buoyant outflow undergoes several stages of adjustment (e.g., Horner-Devine et al., 2015) and ultimately forms a semi-geostrophic coastal buoyancy current propagating downstream along the coastline (e.g., Garvine, 1995). In many theoretical treatments, the freshwater transport through the estuarine mouth and in the coastal buoyancy current are assumed to be equal (e.g., Yankovsky and Chapman, 1997; Lentz and Helfrich, 2002; Whitney and Garvine, 2005).

Mixing of the Dnipro-Buh plume occurs almost entirely on the shelf, so that the resulting coastal buoyancy-driven current is likely to transport downstream only a fraction of the freshwater discharge feeding it. The rest can be transported in the opposite direction by a compensating countercurrent branch propagating upstream and thus maintaining the mass balance on the shelf. This possible two-directional freshwater transport is not the only conspicuous dynamical feature of the Dnipro-Buh plume. Many river plumes are characterized by the formation of the anticyclonic bulge at the estuary mouth. Several studies address various aspects of the bulge dynamics (e.g., O'Donnell, 1990; Yankovsky and Chapman, 1997; Nof and Pichevin, 2001; Avicola and Huq, 2003) and they typically assume a near normal estuarine axis (and hence, outflow) with respect to the coastline orientation. On the other hand, the longitudinal axis of the Dnipro-Buh estuary runs parallel with the coastline downstream (Fig. 1), which is a very unusual configuration.

Propagation of a coastal plume is strongly affected by the wind forcing. The most commonly considered factor is the cross-shore Ekman transport driven by the alongshore wind stress component. For the downwelling-favorable wind (blowing downstream parallel with the coastline), the plume is trapped closer to the coast and propagates faster in the downstream direction than in the unforced case (e.g., Moffat and Lentz, 2012). Conversely, under the upwelling-favorable wind (blowing upstream along the coastline) the plume spreads offshore beyond its unforced limit and sometimes reverses the direction of alongshore propagation (e.g., Berdeal et al., 2002). However, the Ekman dynamics does not operate on the inner shelf, with the Ekman number exceeding one. In this case, the buoyant flow can propagate downwind (e.g., Lentz and Fewings, 2012). Lastly, changing orientation of the coastline can cause a setup of the alongshore pressure gradient which typically counteracts the wind stress (e.g., Crépon et al., 1984). Perhaps surprisingly, light winds can be as efficient as strong winds in transporting buoyant water offshore (e.g., Yankovsky and Yankovsky, 2024).

In this study, we present results of two hydrographic surveys on NWS conducted in May of 1992 and 1994. To the best of our knowledge, their results have not been reported in a peer-reviewed literature. While surveys were not specifically designed to sample the plume, they provide a useful insight into its structure. Moreover, they were conducted under light and variable winds, so that the inherent plume dynamics are likely to be evident. These surveys are complemented with several satellite images of the area obtained at later times, showing plume extension under variable forcing conditions. These images are analyzed in relation to the observed buoyancy and wind forcing. Together, the in-situ measurements and satellite imagery allow us to draw some conclusions about the Dnipro-Buh plume spreading. The rest of the paper is organized as follows. Section 2 describes the data. Section 3 presents results of the data analysis and interprets them in the context of plume dynamics, while section 4 discusses our findings and concludes this study.

2. Observational data

Oceanographic surveys were conducted on 19-21 May 1992 (Fig. 2a) from R/V Trepang and on 12-14 May 1994 (Fig. 2b) from R/V Hydrooptic by Marine Hydrophysical Institute (MHI) of the Ukrainian National Academy of Sciences. Seawater properties were sampled with CTD probe designed and manufactured at MHI. This instrument was extensively tested against SBE CTDs during international research projects (e.g., ComsBlack-93, -94 and TU Black Sea) and showed very good intercalibration results (Oguz et al., 1993; Ivanov et al., 1998). Continuously sampled data were gridded into 1-m vertical bins starting with near-surface measurements referenced at 0 m. Survey data are visualized as horizontal maps and vertical transects using the ODV (Ocean Data View, https://odv.awi.de/en/software/download/) software package and utilizing its built-in module DIVA (Data-Interpolating Variational Analysis) (Schlitzer, 2020).

Satellite observations of plumes on NWS are possible in the visible band because of the regional correlation between the surface water salinity and its optical properties (Bol'shakov, 1970; Grishin and Ilyin, 1983; Ilyin and Grishin, 1988). Satellite images in the visible band were not available for the period of shipboard measurements. Instead, we selected several representative cloud-free MODIS images obtained from Terra and Aqua satellites in 2003 and 2005 (https://worldview.earthdata.nasa.gov/) for the May-June time interval corresponding to the highest climatological freshwater discharge (Ilyin, 2023). All images were color-enhanced by means of an automatic histogram equalization (free image processing software Paint.net) to ensure the best plume water manifestation.

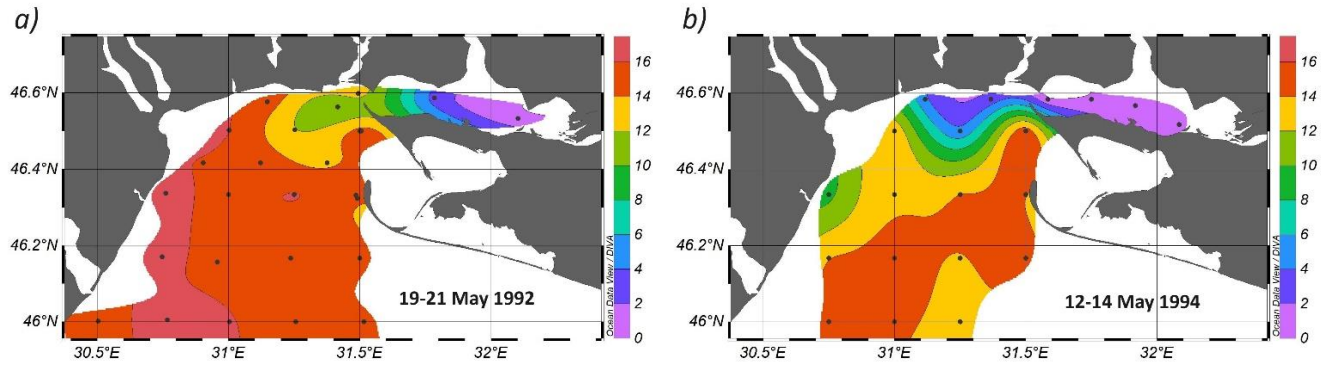

Figure 2. Surface salinity [psu] sampled in (a) 1992 and (b) 1994. Black dots are hydrographic stations.

Auxiliary data for both shipboard and satellite measurements include freshwater discharge, wind velocity, sea level and coastal salinity records. Wind, sea level and coastal salinity measurements were obtained at three hydrometeorological stations: Ochakiv (estuarine mouth), Yuzhniy, and Odesa (both are downstream from the mouth, Figure 1). Daily averaged discharges for both rivers are from the downstream-most streamflow gauges: Kakhovka for the Dnipro River (Nova Kakhovka Hydropower Plant) and Alexandrovka for the P. Buh River (Fig. 1).

3. Results

3.1. Oceanographic surveys

Surface salinity fields corresponding to two surveys are shown in Figure 2 and reveal a rapid offshore spreading of buoyant water westward (downstream) from the estuarine mouth with the formation of a well pronounced bulge. The salinity anomaly of the Dnipro-Buh plume is smaller in 1992: the brackish water occupies the western part of the estuary and the surface salinity s exceeds 12 psu at the mouth. In 1994, all stations in the estuary reveal $s \leq 2$ psu at the surface, with the plume extending farther offshore and downstream on NWS compared to 1992. In 1994, there is a continuity of low salinity water along the NWS coast with the local minimum of s~10

psu in its western part, which can originate from another river discharge, the Dniester River or even the Danube River.

Vertical transects further corroborate the Dnipro-Buh plume structure (Figures 3 and 4). In both years, the buoyant layer detaches from the bottom well within the estuary, roughly halfway between its head (where the Dnipro River runs off), and the mouth, which is typical of salt wedge estuaries. Subsequently, the plume spreads as a thin, 2-4 m deep layer. Stratification is sustained mainly by salinity but temperature also contributes, and the ambient shelf water with $s \geq 17$ psu penetrates to the mouth in the bottom layer. The average depth of the Dnipro estuary is 4.3 m, and of its mouth is 4.4 m (Ilyin, 2023). In both years, hydrographic surveys were conducted along the estuarine thalweg (a navigation channel). This channel acts as a conduit for relatively cold and saline ambient shelf water entering the estuary so that the halocline lies at or below the average depth of the Dnipro-Buh estuary (Ilyin, 2023).

Different extensions of the buoyant layer between the two surveys can be related to different freshwater discharge conditions preceding surveys (Fig. 5). In 1992, the average discharge during 7-21 May (time interval shown in Figure 5) was 1386 m^3s^{-1}, while during the first half of May 1994 it was 3293 m^3s^{-1}, that is, ~2.4 times higher. Also, temporal trends prior to surveys were opposite in those years: in 1992 the discharge was falling after peaking at 1535 m^3s^{-1} on 12 May, while in 1994 it sharply increased from ~3150 m^3s^{-1} to more than 3500 m^3s^{-1} over a two-day time interval, on 9-11 May.

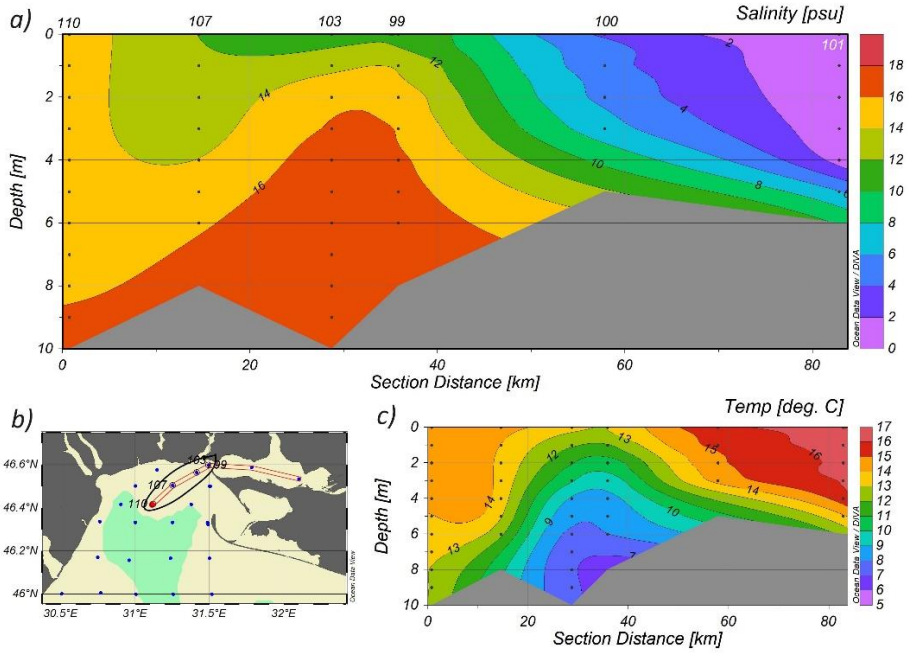

Figure 3. Vertical transects of (a) salinity and (c) temperature in 1992, with station numbers shown at the top of panel (a). The transect is denoted with red lines on the map in panel (b), where green shading represents water depth exceeding 10 m.

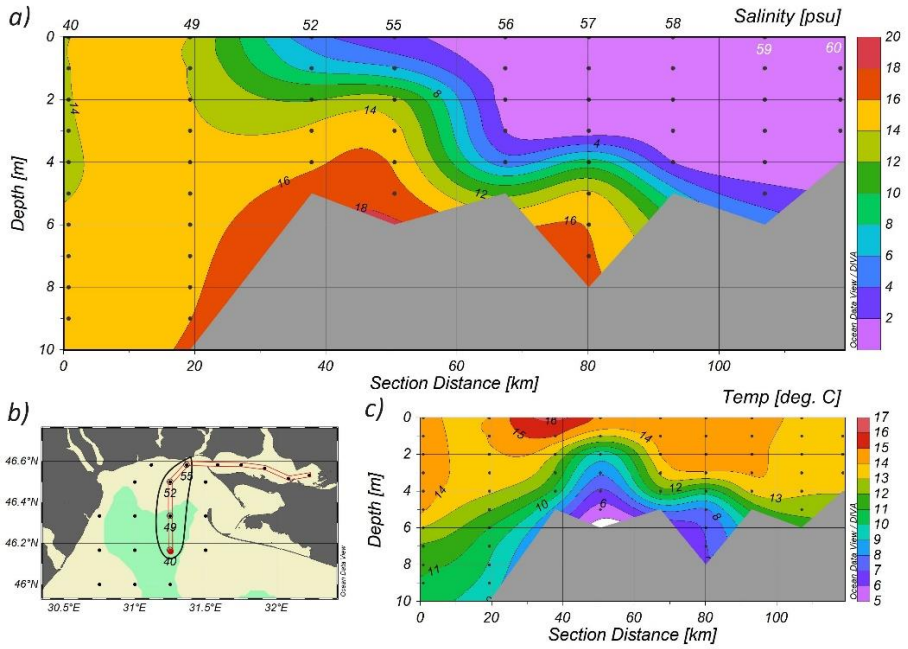

154

155 **Figure 4**. Same as in Figure 3, but for the 1994 survey.

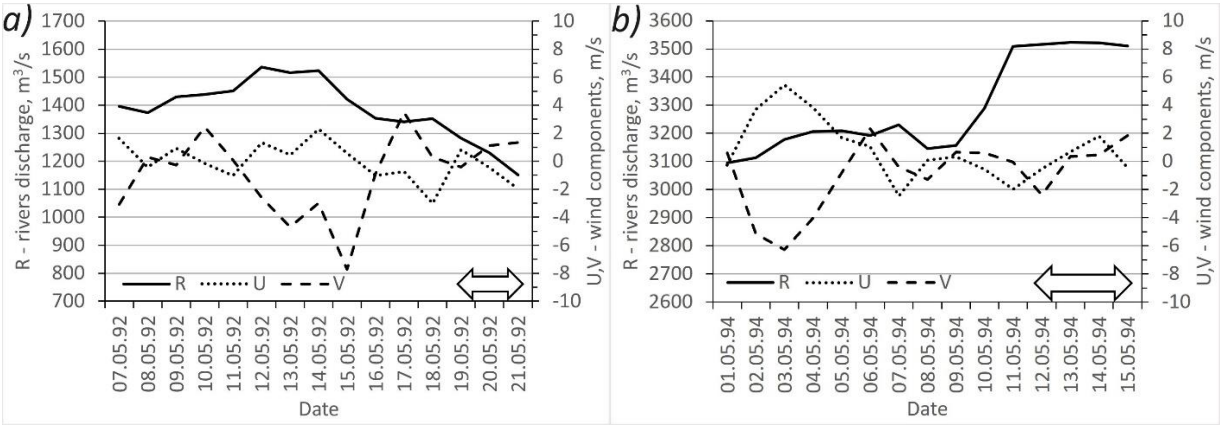

156

157 **Figure 5**. Time series of the combined Dnipro – P. Buh freshwater discharge (solid line), zonal (dotted line) and
158 meridional (dashed line) wind components measured at Ochakiv station for (a) 1992 survey, and (b) 1994
159 survey. Survey time period is shown with a double arrow symbol.

160 Transport of buoyant water within the plume is sustained by both its inherent dynamics (presumably
161 geostrophic), and by external forcing, associated predominantly with the wind stress. In order to assess a
162 relative role of the inherent plume dynamics, we estimate a geostrophic transport of freshwater around the
163 bulge and compare it to freshwater discharge feeding the plume. Geostrophic balance is considered to
164 represent the leading-order dynamics in the unforced far field of a plume, and the freshwater transport in the
165 far field should match closely the freshwater discharge if the plume is in near-stationary conditions. This
166 estimate is performed for the 1992 survey through transect comprising stations 99, 103, 107 and 110 (Fig. 3),
167 and for the 1994 survey through transect formed by stations 40, 49, 52 and 55 (Fig. 4). Stations comprising the
168 1992 transect were occupied within the 24 h time period (late 19 May – late 20 May), while in 1994 this time
169 interval was slightly longer, 26-27 h (late 12 May through 13 May). Given the non-tidal nature of the Black Sea

and light winds in both years, we consider these transects as synoptic for calculating a geostrophic transport. The net geostrophic transport depends on the difference of buoyancy characteristics in the center of the plume and outside (ambient shelf water), which are both resolved. The results of these estimates are summarized in Table 1.

Since the water column is continuously stratified without a well-defined interface between the plume and ambient shelf waters, we estimate the depth of buoyant layer *h* following Arneborg et al. (2007) as:

$$h = \frac{2\int_{-D}^{0}(\rho_0-\rho)z\,dz}{\int_{-D}^{0}(\rho_0-\rho)\,dz} \qquad (1),$$

where $\rho(z)$ is the seawater density and ρ_0 is the reference density, which is a maximum (near bottom) value at each station, *D* is the water depth, and the vertical coordinate *z* points upward. We also estimate the equivalent freshwater layer depth h_f as:

$$h_f = \int_{-D}^{0}\frac{s_r-s}{s_r}\,dz \qquad (2),$$

where s_r=17 is the reference salinity representing ambient water on the shelf.

The freshwater layer is deeper in 1994 (Table 1), which is consistent with higher freshwater discharge in that year. Interestingly, h_f does not decrease with the offshore distance: even though the salinity anomaly of the buoyant layer decreases, its depth increases, so that the freshwater content remains roughly the same. This feature indicates that effective mechanisms for the offshore dispersal and mixing of buoyant water are in action.

The freshwater content yields a straightforward estimate of the baroclinic Rossby radius $Rd_i = \sqrt{g'h_f}/f$, where g'=0.132 ms^{-2} is the reduced gravity associated with the freshwater density anomaly relative to the ambient salinity of 17 psu (temperature variations are ignored), and f=1.06×10^{-4} s^{-1} is the Coriolis parameter. For station 52 in the 1994 survey (Fig. 4), $Rd_i \approx$ 4.8 km. Due to a coarse spatial resolution, it is difficult to demarcate the exact offshore position of the plume, but it is more than 30 km (Fig. 4) and hence exceeds Rd_i by a factor of 6 or more. Previously, Yankovsky and Chapman (1997) derived the offshore scale for an anticyclonic bulge in the gradient wind balance equal to ~4.2Rd_i, while Lentz and Helfrich (2002) posited that in the far field of the buoyancy current the front outcrops offshore from the bottom over the Rd_i distance. Clearly, the Dnipro-Buh plume during the 1994 survey extended offshore beyond those length scales.

Table 1. Plume characteristics derived from hydrographic surveys in 1992 and 1994 (see Figures 3 and 4, respectively, for station locations): *h* [m] is the buoyant layer depth from (1), h_f [m] is the equivalent freshwater layer depth from (2), Q_g [m^{3}s^{-1}] is the freshwater geostrophic transport from (4), positive eastward.

Survey 1992

Station	*h*	h_f	Q_g
99	1.47	0.54	108
103	2.99	0.95	136
107	4.01	1.39	-296
110	10.21	0.98	

Survey 1994

Station	*h*	h_f	Q_g
55	1.60	1.77	-65
52	1.67	1.94	-769
49	8.43	1.38	508
40	10.80	1.91	

Next, we calculate a baroclinic geostrophic velocity by integrating the thermal wind shear equation upward from the reference level. As a reference level for a pair of stations, we select the closest to *h* grid point (typically, below *h*) at the inshore station. The thermal wind shear is:

$$\frac{\partial u_g}{\partial z} = \frac{g}{f\rho}\frac{\partial \rho}{\partial y} \quad (3)$$

Here, u_g is the geostrophic velocity component normal to the transect (positive upstream/eastward) and *g* is the acceleration due to gravity.

Finally, we calculate the freshwater transport by a geostrophic current as:

$$Q_g = \int_{-h}^{0} u_g \frac{s_r - s}{s_r} dz \quad (4)$$

For 1992, the negative (westward) geostrophic transport of freshwater occurs only in the outer part of the plume, between stations 107 and 110, and totals 296 $m^3 s^{-1}$, which is significantly less than the combined Dnipro-Buh freshwater discharge of ~1350-1500 $m^3 s^{-1}$ before the survey (Fig. 5a). The inshore part of the transect (stations 99-103-107) reveals the eastward geostrophic freshwater transport totaling 244 $m^3 s^{-1}$. Thus, the net freshwater transport by geostrophic circulation through the whole transect is merely -52 $m^3 s^{-1}$, suggesting that other processes might be responsible for the offshore and downstream spreading of buoyant water. This number also implies that a significant fraction of the freshwater outflow can recirculate within the bulge or propagate upstream.

In 1994, the freshwater discharge was higher (~3200-3500 $m^3 s^{-1}$, Figure 5b), which resulted in a larger plume with lower salinity. The total downstream (westward) geostrophic transport of freshwater between station 55-52-49 is 834 $m^3 s^{-1}$; which is roughly a quarter of the riverine freshwater runoff. The offshore pair of stations on this transect, stations 49-40, exhibit the upstream freshwater transport of 508 $m^3 s^{-1}$, with the net downstream freshwater transport through the transect totaling 327 $m^3 s^{-1}$. It should be noted that the buoyant layer depth *h* derived from (1) roughly corresponds to the reversal of the thermal wind shear at outer stations on analyzed transects, where the downstream geostrophic transport concentrates. For instance, in 1994 at station 52 the buoyant layer depth is ~1.7 m. Between this station and 49 (lying farther offshore) the isohalines outcrop in the uppermost 2 m layer, and deepen below (Fig. 4), indicating the reversal of the horizontal density gradient, and consequently, of the geostrophic velocity shear. A similar tendency is seen in the 1992 survey between stations 107 (h≈4m) and 110, although in this case the density gradient reversal is in part due to the thermal gradient below 4 m (Fig.3).

Thus, in both years the downstream geostrophic transport of freshwater typical for large, rotational plumes is only a small fraction of the riverine discharge, which implies that a substantial amount of freshwater can be transported upstream through the development of a two-layer circulation associated with the plume mixing. Although in many cases the upwelling-favorable wind prevents the downstream propagation of buoyant water in a geostrophicly-adjusted plume, no such events were registered in wind records around the time of both surveys (Fig. 5). In 1992, a relatively strong wind event occurred on 13-15 May, when the wind was predominantly offshore (southward), but with some eastward (upstream) component. Such a wind forcing should be favorable for the offshore detachment of a plume and for the westward Ekman transport farther offshore, over deeper water. Indeed, salinity records at both Ochakiv (estuarine mouth) and Yuzhniy (33 km downstream) indicate salinity increase during this event (Fig. 6a). Subsequently, the wind relaxed and remained light through the survey period, while the salinity remained high at Yuzhniy (s≈14-16 psu), and slightly subsided

at Ochakiv to less than 4 psu. In 1994, a somewhat similar wind event occurred earlier in time (relative to the survey period), around 2-5 May. In this case, the upstream and offshore wind components were more comparable (that is, northwesterly wind in meteorological notation). Again, this wind event was followed by an abrupt increase of salinity at Yuzhniy to s>16 psu (close to an ambient shelf salinity outside of the plume) (Fig. 6b). Once the wind relaxed, the salinity subsided to s≈8 psu over the next two days (by 8 May). As in 1992, the wind was light and variable immediately prior to and during the survey. Unlike 1992, salinity was consistently low at Ochakiv, maintaining a constant value of s=2 psu, likely due to a higher freshwater discharge.

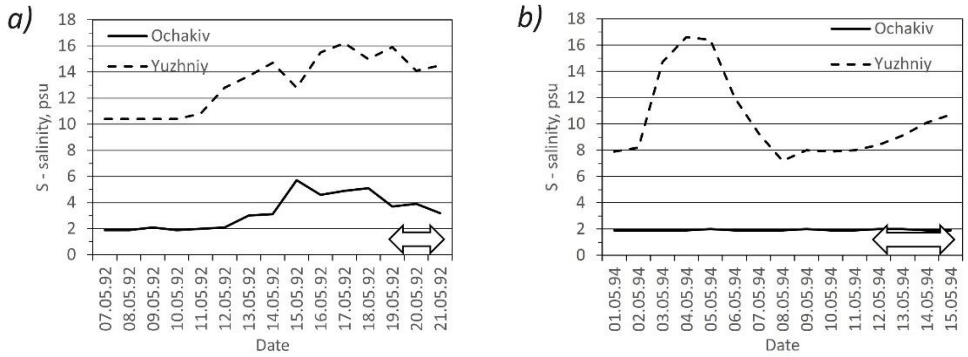

Figure 6. Nearshore salinity records at stations Ochakiv and Yuzhniy in (a) May 1992, and (b) May 1994.

To better assess the role of wind in the evolution of the Dnipro-Buh plume, we will quantify a relative contribution of the buoyancy and wind forcing in the coastal current formation by using the sea level data. We start with buoyant outflow, which, in the absence of other forcing agents, should form a geostrophic coastal current propagating alongshore. If the buoyancy is conserved (a frequently made assumption, as was mentioned in the introduction), the maximum depth h_b of this current can be defined (Yankovsky and Chapman, 1997) as:

$$h_b = \sqrt{2Qf/g'} \qquad (5)$$

Assuming that the average salinity of the buoyancy current is s_p and the density is a function of salinity only, the volumetric transport of the buoyancy current Q and its associated reduced gravity g' can be defined as:

$$Q = \frac{Q_r s_r}{\Delta s} \quad \text{and} \quad g' = \frac{g\gamma\Delta s}{\rho_0} \qquad (6),$$

where $\Delta s = s_r - s_p$ and Q_r is the river discharge feeding the plume. Next, we assume that the cross-sectional area of the buoyancy current is a triangle, with the linear bottom and straight frontal interface outcropping from h_b to the surface. This is the same geometry adopted by Lentz and Helfrich (2002). With this, Q is defined as:

$$Q = \frac{1}{2} h_b \int_{-L_p}^{0} \bar{u} dy = \frac{1}{4} h_b \int_{-L_p}^{0} u_s dy \qquad (7)$$

Here $\bar{u}$ and u_s are depth-averaged and surface velocity x-components, respectively; x- and y-axes point east- and northward, zonal coastline is at y=0, and L_p is the plume width. Lastly, u_s is in geostrophic balance $u_s = -\frac{g}{f}\frac{\partial \eta}{\partial y}$, where η is the free surface perturbation, $\eta = \eta_0$ (y=0) and $\eta = 0$ (y=-L_p). Substituting the expression for u_s into (7), integrating and assuming westward Q yields:

$$\eta_0 = \frac{4Qf}{g h_b} = \sqrt{\frac{8 Q_r f \gamma s_r}{g \rho_0}} \qquad (8)$$

Expression (8) is the scale for the free surface perturbation at the coast if the geostrophic coastal current was formed and carried all discharged water downstream along the coast. Interestingly, this scale depends on the freshwater discharge Q_r and the density difference between the fresh and ambient ocean water γs_r, but it does not depend on the extent of mixing between the plume and the shelf water Δs (while both Q and h_b do).

Figure 7 shows the dependence of η_0 on freshwater discharge assuming γ=0.78 kg m^{-3} (appropriate for the range of salinity observed on NWS), f=1.06×10^{-4} s^{-1}, ρ_0 =1014 kg m^{-3}, and s_r =17 psu. Next, we compare this scale for buoyancy forcing with the observed sea level: we take a standard deviation σ of daily-averaged sea level at three locations shown in Figure 1 (Ochakiv, Yuzhniy and Odesa) over the same 15-day time interval as in Figure 5. Daily averaging retains only subinertial oscillations and eliminates inertial-gravity waves (e.g., seiches). The results are also shown in Figure 7, where σ is plotted over the range of Q_r observed during the corresponding 15-day time intervals. It should be noted that σ represents mostly the wind-driven dynamics (since wind changed direction over the analyzed period), but can also contain a signal associated with the buoyancy current mesoscale variability, resulting for instance from its baroclinic instability. In both years, σ at Ochakiv (estuarine mouth) was below the estimated η_0 in the buoyancy current. This implies that wind forcing was not sufficiently strong to disrupt the formation of the buoyancy-driven coastal current. In 1992, σ increased downstream (from Ochakiv to Odesa), which can be associated with generation of subinertial coastally trapped waves (CTWs) on sub-basin or even basin scales. CTWs propagate only downstream (same as Kelvin waves) and as they encounter an abruptly widening shelf (NWS), they form a shadow zone near the coast immediately downstream of the shelf width discontinuity (e.g., Wilkin and Chapman, 1987; Yankovsky and Chapman, 1995). Farther downstream, CTW amplitude increases both due to the incident wave adjustment and due to its scattering into other (typically, higher) modes. From visual evaluation of sea level records (not shown), it appears that CTW pulse with variable amplitude alongshore was associated with a stronger wind event around 15 May 1992. In 1994, the coastal response to wind forcing was more local, and was nearly identical at all three locations (Fig. 7).

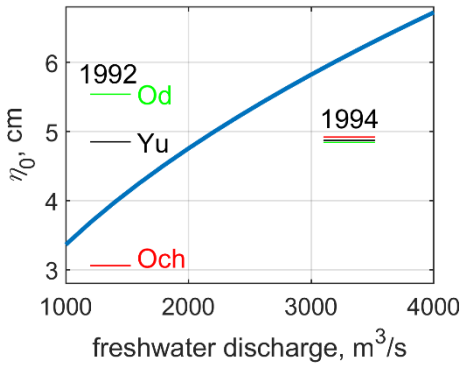

Figure 7. Estimate of a coastal sea level perturbation associated with the geostrophic buoyancy current (heavy blue line) and the observed sea level standard deviations at Ochakiv (red), Yuzhniy (black), and Odesa (green) shown over the freshwater discharge range for a corresponding year.

Overall, during both surveys the Dnipro-Buh plume was observed under light wind conditions such that the plume dynamics should dominate the wind-induced sea level setup and corresponding barotropic transport. Under this scenario, our estimates indicate that only a fraction of total freshwater discharge was transported downstream in geostrophic buoyancy driven current around the bulge. A significant amount of freshwater was contained in the bottom layer which likely propagated in the opposite, upstream direction, as deduced from the thermal wind shear reversal. Also, due to a coarse spatial resolution of both surveys, the role of subemeso- and

meso-scale processes in freshwater transport is unknown. Lastly, the analyzed surveys did not extend eastward from the mouth's longitude (except for the estuary itself) and hence the freshwater content in that part of NWS is unknown. To better illustrate the pathways of the Dnipro-Buh freshwater outflow, in the next subsection we consider a set of satellite images obtained under similar conditions of spring freshet, with a variety of wind and discharge patterns, which demonstrate a bi-modal spreading of the Dnipro-Buh river plume.

3.2. Satellite imagery

Per Dnipro-Buh estuary climatology (Ilyin, 2023), maximum riverine discharge occurs anytime from late April through early June but typically in May, thus the "classical" plume structure can be observed from space in these months, especially during low-wind conditions or light easterly winds sustaining the westward transport alongshore. A common approach consists of using the spatial and spectral contrasts between the marine waters of different origin in high- and medium-resolution satellite imagery to visualize the coastal dynamics features. Plumes of buoyant water produced by riverine discharge through the river deltas and estuaries are the most convenient objects for the satellite observations. Based on the previous studies (Ilyin, 1999, 2023), we identify changes in plume's configuration on sequential satellite imagery in order to obtain qualitative and some quantitative description of the Dnipro-Buh plume evolution.

The first series of images discussed here was obtained on 27 May through 13 June 2003 (Figures 8 and 9). On 27 May, the plume extends both downstream (westward) and upstream (southeastward) from the mouth. Interestingly, the upstream part of the plume appears to be less diffuse than its downstream counterpart, and has a well-pronounced near-circular, eddy-like leading edge. Also, a sharper color signature of the upstream part can be linked to a lesser diluted estuarine outflow, which implies that the initial advection of buoyant water from the mouth occurs in the upstream direction. Subsequently, the buoyancy-driven flow executes anticyclonic turn around the leading edge, and continues downstream at some offshore distance, in a close proximity to the offshore tip of Tendra Spit (Fig. 8a). This overall pattern is reminiscent of several earlier idealized modeling studies about the upstream propagation of the coastal buoyant plume (e.g., McCreary et al., 1997; Yankovsky, 2000; Matano and Palma, 2010), and was also reported in a recent modeling study by Brasseale and MacCready (2021) addressing the mixing-driven two-layer plume dynamics and utilizing more advanced numerical tools. The plume was forced by lower-than-climatological freshwater discharge of ~800-900 m^3s^{-1} (Fig. 9a). The alongshore wind component reversed from westward to eastward approximately three days before the image was taken (Fig. a), and the response in the coastal salinity record to this reversal is clearly seen as a local salinity maximum at Yuzhnyi lagging by approximately one day (Fig. 8b). Thus, wind could contribute to the upstream advection of the plume, but the intrinsic plume dynamics was likely to play a role, too, since the wind was light (2-3 ms^{-1}) prior to the time of the image.

The next image taken 5 days later (on 1 June) reveals the coastal water occupying the whole northernmost part of NWS. The frontal zone between greenish coastal and dark-blue offshore waters exhibits rich mesoscale dynamics with frontal eddies of various scales, implying that the rotational effects are of the leading order. However, there is no resemblance of typical coastal plume comprising a bulge and a narrower coastal current. The wind prior to this image was again light and variable switching from southwesterly to northeasterly.

The last three images in this series from 8 through 13 June (Fig. 8c-e) show that the coastal buoyant water was trapped in the eastern part of NWS, which is also evident in the increasing salinity $s \geq 16$ psu at both Yuzhnyi and Odessa around this time (Fig. 9b). Note that the meridional wind component was consistently northward for almost one week supporting the eastward Ekman transport on the shelf (Fig. 9a). In addition, an upwelling-

favorable wind event occurred before and during the last image' time (the eastward wind component peaking above 5 ms^{-1}, Fig. 9a) resulting in the southward advection of plume water from the area of Tendra Spit (Fig. 8e).

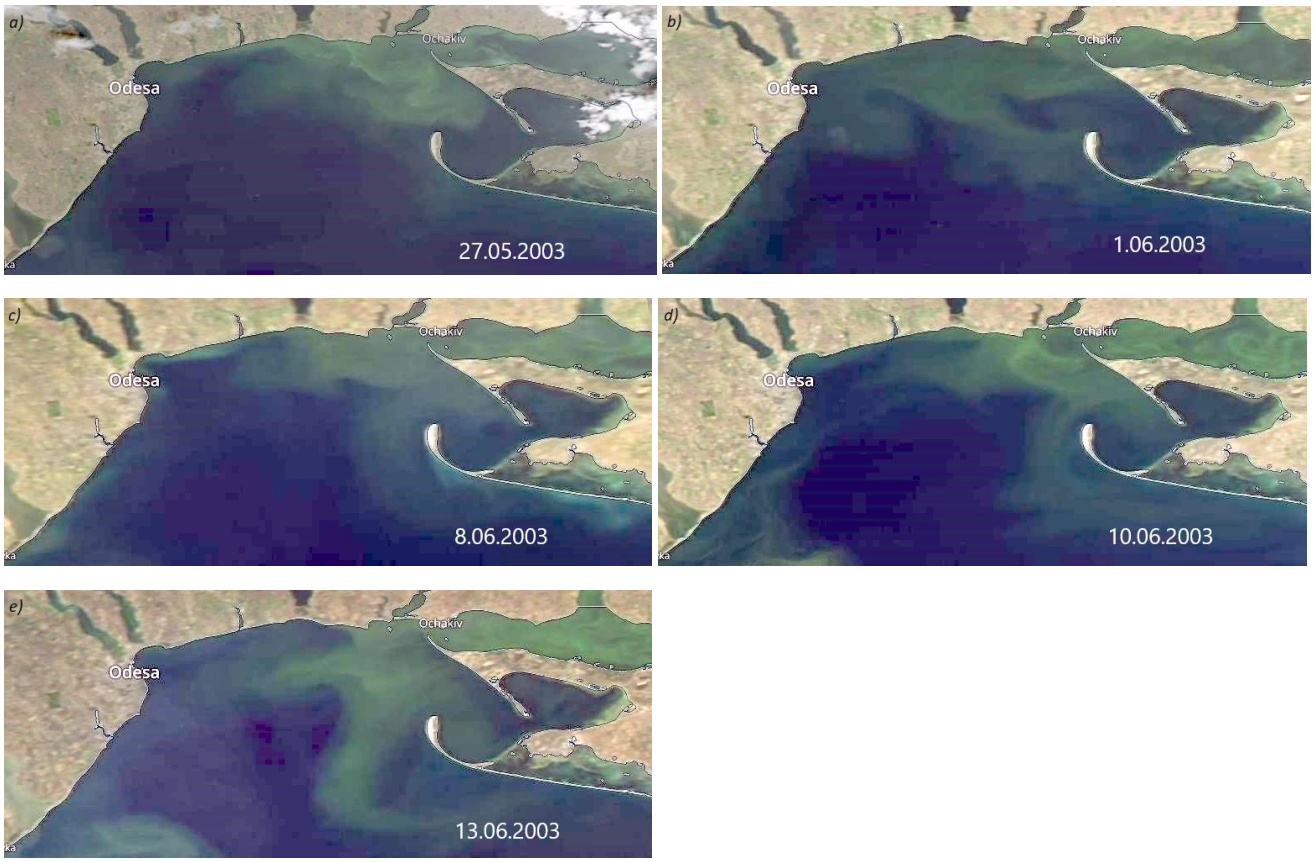

Figure 8. Aqua MODIS enhanced natural color images of NWS obtained on (a) 27 May, (b) 1 June, (c) 8 June, (d) 10 June, (e) 13 June, 2003.

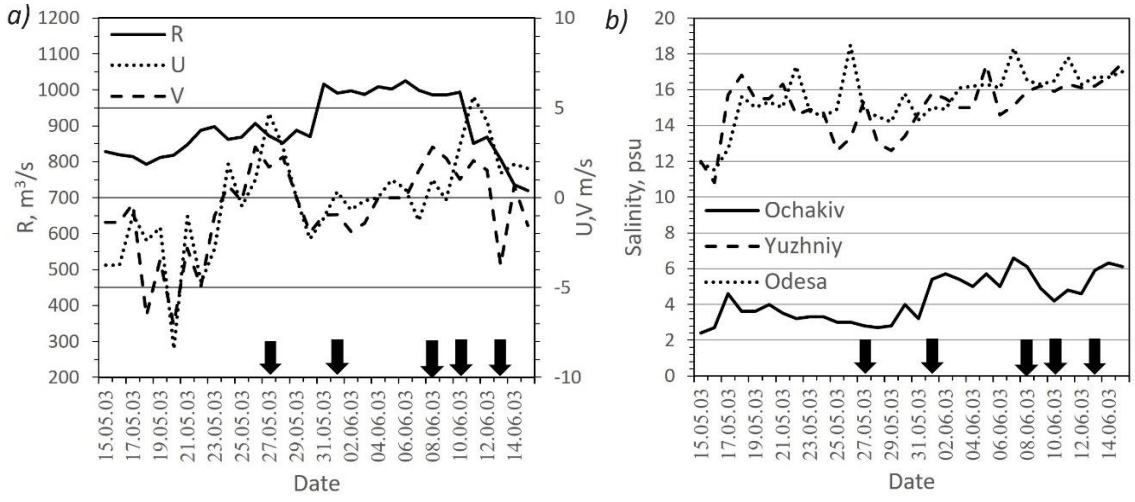

Figure 9. Time series (a) as in Figure 5, and (b) as in Figure 6 but for three hydrometeorological stations; May-June 2003. Black arrows represent times of satellite images.

Overall, the rotational (geostrophic) dynamics is evident in series of images in numerous vortical frontal structures, but there was no pronounced anticyclonic bulge near the mouth. The plume appeared to be sensitive to the wind forcing, since its shape followed wind changes, and the wind could suppress the formation of a bulge, especially since the freshwater discharge was low.

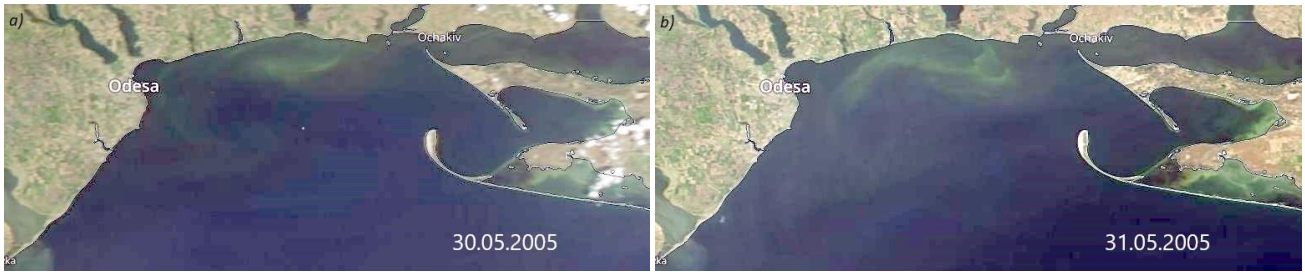

Figure 10. Same as in Figure 8, but for (a) 30 May, and (b) 31 May 2005.

The second subset of images is from 30-31 May 2005 (Figures 10 and 11). These two satellite images reveal a structure resembling typical rotational plume: an anticyclonic bulge extending offshore and continuing downstream toward Odessa as a narrower coastal current. This plume structure is particularly obvious on May 31 (Fig. 10b), and is highlighted by a streak of light-green color: a semi-circle with a detached filament extending downstream roughly parallel with the coast. Light green color might be associated with a high concentration of phytoplankton due to frontal convergence. The bulge is elongated and is swept downstream from the mouth due to the prolonged action of westward (downwelling-favorable) wind component lasting for more than a week prior to time of images (Fig. 11a). This trend was further assisted by the southward pulse of meridional wind component peaking two days prior to the first image and causing a westward Ekman drift. The downwelling-favorable wind action resulted in a coastal salinity drop to < 5 psu at Yuzhniy on 27 May and to ~8 psu at Odessa a day later. The plume was fed by a higher-than-climatological discharge, already reaching ≈2200 m^3s^{-1} in mid-May and rapidly increasing to ≈2600 m^3s^{-1} between 25-27 May. Overall, the observed plume is in good agreement with the expected structure of rotational plume affected by the light downwelling-favorable wind.

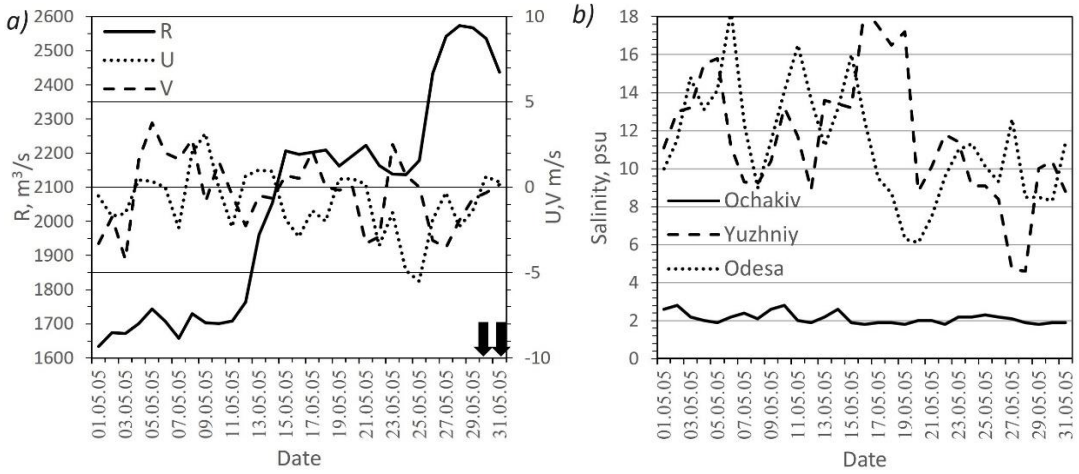

Figure 11. Same as in Figure 9, but for May 2005.

4. Discussion and conclusions

Both in situ and remote observations presented here demonstrate that the Dnipro-Buh plume does not form a geostrophic coastal current carrying most of the freshwater discharge downstream, unless assisted by the downwelling-favorable wind (as seen in the 2005 example). Series of satellite images from 2003 show a significant penetration of the plume water upstream from the mouth, in the southeastward direction, under the influence of light and variable winds. There are several plumes worldwide with well documented bimodal propagation along the coast, both downstream (a natural pathway) and upstream. Examples include the Columbia River plume (e.g., Hickey et al., 2009), the Rio de la Plata plume (e.g., Bodnariuk et al., 2021), and the Changjiang (Yangtze) River plume (e.g., Wu and Wu, 2018). In these examples, there is substantial tidal mixing and the upstream spreading is observed during the summer season (austral summer for the Rio de la Plata plume), under the influence of persistent upwelling favorable winds. In particular, Wu and Wu (2018) conducted several numerical experiments to demonstrate that tidal mixing supports the formation of the downstream propagating coastal current and in this way resists the diversion of buoyant water by wind both upstream and offshore.

Previous idealized modeling studies repeatedly demonstrated that a fraction of the estuarine buoyant outflow on the shelf can propagate upstream from the mouth without wind forcing. This process appears to be controlled by the shelf mixing and the rotational adjustment of the buoyant outflow (e.g., McCreary et al., 1997; Yankovsky, 2000; Matano and Palma, 2010), although some numerical artifacts in earlier models could amplify this trend (e.g., Yankovsky, 2000; Garvine, 2001). However, the upstream spreading is a robust feature of newer numerical experiments with realistic representation of the estuarine-shelf continuum and the state-of-the-art mixing parameterization on the shelf (e.g., Brasseale and MacCready, 2021). The upstream spreading also implies detachment of the buoyant layer from the frictional bottom, which is a common feature of all numerical models simulating this process. This natural upstream propagation is difficult to detect in observations, because it is masked by other processes occurring on the shelf and unrelated to the freshwater discharge, such as wind stress, alongshelf pressure gradient, residual tidal currents, offshore forcing, etc. Nevertheless, significant upstream spreading of the Dnipro-Buh plume observed on May 27 (Fig. 8a) occurred without persistent upwelling winds, suggesting that the intrinsic plume dynamics could be at least partially responsible for the observed pattern.

Within the Dnipro-Buh plume area, both temperature and salinity change continuously with depth, without a well-defined interface between the plume and the ambient shelf water. Estimates of the buoyant layer thickness under such conditions agree well with the depth where the horizontal density gradient sign (and hence, the sign of the thermal wind shear) reverses. This implies that a significant fraction of freshwater discharge is trapped in the bottom and/or offshore layer recirculating around the bulge in the direction opposite to the surface buoyancy driven current. Unlike the thin, surface-advected Dnipro Buh plume itself, the return flow is controlled by the frictional bottom in the manner of the arrested topographic wave solution by Csanady (1978), as was recently demonstrated by Brasseale and MacCready (2021). Overall, the plume dynamics appears to be sensitive to the wind-driven shelf circulation (its effect includes both straining and depth-averaged advection) and is further complicated by the development of various frontal instabilities. Meso- and submesoscale processes are particularly active here due to the absence of the tidally-driven bottom boundary layer, as well as predominantly light winds during the observations reported here. Possible nature of such instabilities has been extensively discussed in several recent modeling studies (e.g., Ayouche et al., 2020; Lv et al., 2020; Ayouche et al., 2021; Brink, 2024; Yankovsky and Yankovsky, 2024).

In conclusion, lack of tidal mixing in the Dnipro-Buh estuary leads to the formation of a thin, 1.5-3 m deep surface-advected plume with an initially strong salinity anomaly and small volumetric transport. The estuarine

outflow runs off parallel with the coastline, but it rapidly widens with downstream distance expanding offshore over multiple baroclinic Rossby radii, beyond the typical limits for geostrophic coastal plumes. On synoptic to monthly time scales, the Dnipro-Buh plume spreads in bimodal fashion, so that the buoyant water is present both upstream and downstream from the estuarine mouth. Geostrophic transport of freshwater in the plume is a small fraction of the freshwater discharge feeding the plume, while the buoyant layer rapidly responds to wind variations. Also, as salinity anomaly decreases offshore, the freshwater content remains near-constant or even increases. This implies that the freshwater spreading is sustained by cross-frontal "diffusion" to a greater extent than through the advection by geostrophic circulation associated with the plume. This "diffusion" likely results from advection by relatively light winds combined with meso- and submesoscale instabilities in the frontal region. Processes controlling a vertical mixing and a lateral spreading of the Dnipro-Buh plume merit further investigation.

Acknowledgements. AY was supported by the US National Science Foundation grant OCE-2148480; YI was supported by the state funding of Ukraine under the research project No 0122U002444. We are thankful to Dr. Preston Spicer and an anonymous reviewer for their insightful comments and suggestions.

References

Arneborg, L., Fiekas, V., Umlauf, L., Burchard, H., 2007. Gravity current dynamics and entrainment - A process study based on observations in the Arkona Basin. J. Phys. Oceanogr. 37, 2094–2113. https://doi.org/10.1175/JPO3110.1

Avicola, G., Huq, P., 2003. The characteristics of the recirculating bulge region in coastal buoyant outflows. J. Marine Res. 61, 435-463.

Ayouche, A., Carton, X., Charria, G., Theettens, S., Ayoub, N., 2020. Instabilities and vertical mixing in river plumes: Application to the Bay of Biscay. Geophys. Astrophys. Fluid Dyn. 114, 650–689. https://doi.org/10.1080/03091929.2020.1814275.

Ayouche, A., Charria, G., Carton, X., Ayoub, N., Theetten, S., 2021. Non-linear processes in the Gironde River plume (north-east Atlantic): Instabilities and mixing. Front. Mar. Sci. 8, 701773. https://doi.org/10.3389/fmars.2021.701773.

Berdeal, G.I., Hickey, B.M., Kawase, M., 2002. Influence of wind stress and ambient flow on high discharge river plume. J. Geophys. Res. 107C, 3130. doi:10.1029/2001JC000932.

Bol'shakov, V.S., 1970. Transformation of riverine waters in the Black Sea. Kiev, Naukova Dumka, 1970. 328 pp. In Russian

Bodnariuk N., Simionato, C.G., Osman, M., Saraceno, M., 2021. The Río de la Plata plume dynamics over the Southwestern Atlantic Continental Shelf and its link with the large scale atmospheric variability on interannual timescales. Cont. Shelf Res. 212, 104296. https://doi.org/10.1016/j.csr.2020.104296

Brasseale, E., MacCready, P., 2021. The Shelf Sources of Estuarine Inflow. J. Phys. Oceanogr. 51, 2407-2421. DOI: 10.1175/JPO-D-20-0080.1

Brink, K.H., 2024. The effect of alongshore wind stress on a buoyancy current's stability. Cont. Shelf Res. 272, 105149. https://doi.org/10.1016/j.csr.2023.105149

Burchard, H., Lange, X., Klingbeil, K., MacCready, P., 2019. Mixing Estimates for Estuaries. J. Phys. Oceanogr. 49, 631-648. DOI: 10.1175/JPO-D-18-0147.1

Csanady, G.T., 1978. The arrested topographic wave. J. Phys. Oceanogr. 8, 47–62.

Crépon, M., Richez, C., Chartier, M., 1984. Effects of coastline geometry on upwellings. J. Phys. Oceanogr. 14, 1365-1382.

Garvine, R.W., 1995. A dynamical system for classifying buoyant coastal discharges. Cont. Shelf Res. 15, 1585-1596.

Garvine, R.W., 2001. The impact of model configuration in studies of buoyant coastal discharge. J. Marine Res. 59, 193–225.

Geyer, W.R., MacCready, P., 2014. The estuarine circulation. Annu. Rev. Fluid Mech. 46, 175–19. https://doi.org/10.1146/annurev-fluid-010313-141302

Grishin, G.A., Ilyin Y.P., 1983. Variability of oceanographic fields in the northwestern part of the Black Sea based on satellite video data. In: Methods of the Space Oceanographic Information Processing. Sevastopol. 78-83. In Russian.

Hickey, B., McCabe, R., Geier, S., Dever, E., Kachel, N., 2009. Three interacting freshwater plumes in the Northern California Current system. J. Geophys. Res. 114, C00B03. https://doi.org/10.1029/2008JC004907.

Horner-Devine, A.R., Hetland, R.D., MacDonald, D.G., 2015. Mixing and transport in coastal river plumes. Annu. Rev. Fluid Mech. 47, 569–594. https://doi.org/10.1146/annurev-fluid-010313-141408.

Ilyin, Y.P., 1999. Expansion of riverine water. In: Natural conditions of the seaside of the Danube River and the Snake Island / Ivanov V.A., Goshovsky S.V. (editors). Sevastopol: MHI NASU. 5-73. In Russian

Ilyin, Y.P., 2023. Average conditions and seasonal variability of the structure and dynamics of transitional waters in the Dnieper-Bug estuary region. Ukrainian Hydrometeorological Journal 32, 63-79. In Ukrainian. https://doi.org/10.31481/uhmj.32.2023.05

Ilyin Y.P., Grishin G.A., 1988. Summer freshening of the northwestern part of the Black Sea and the possibility of its control by satellite video data / Geographical interpretation of aerospace information. Moscow. 119-125. In Russian

Ivanov L., Konovalov S., Melnikov V., et al., 1998. Physical, chemical and biological data sets of the TU Black Sea data base: description and evaluation / L.I. Ivanov and T. Oguz (eds.) “Ecosystem Modelling as a Management Tool for the Black Sea, vol. 1”. Kluwer AP. 11-37.

Lentz, S.J., Helfrich, K.R., 2002. Buoyant gravity currents along a sloping bottom in a rotating fluid. J. Fluid Mech. 464, 251-278. doi:10.1017/S0022112002008868

Lentz, S. J., Fewings, M. R., 2012. The Wind- and Wave-Driven Inner-Shelf Circulation. Annual Review of Marine Science 4(1), 317–343. https://doi.org/10.1146/annurev-marine-120709-142745

Lv, R., Cheng, P., Gan, J., 2020: Adjustment of river plume fronts during downwelling-favorable wind events. Cont. Shelf Res., 202, 104143, https://doi.org/10.1016/j.csr.2020.104143.

MacCready, P., Geyer, W.R., Burchard, H., 2018. Estuarine exchange flow is related to mixing through the salinity variance budget. J. Phys. Oceanogr**.** 48**,** 1375–1384, https://doi.org/10.1175/JPO-D-17-0266.1.

Matano, R.P., Palma, E.D., 2010. The Upstream Spreading of Bottom-Trapped Plumes. J. Phys. Oceanogr. 40, 1631-1650. DOI: 10.1175/2010JPO4351.1

McCreary, J.P., Zhang, S., Shetye, S.R., 1997. Coastal circulation driven by river outflow in a variable-density 1 1⁄2-layer model. J. Geophys. Res. 102C, 15,535–15,554.

Moffat, C., Lentz, S., 2012. On the Response of a Buoyant Plume to Downwelling-Favorable Wind Stress. J. Phys. Oceanogr. 42, 1083-1098. DOI: 10.1175/JPO-D-11-015.1

Nof, D., Pichevin, T., 2001. The ballooning of outflows. J. Phys. Oceanogr. 31, 3045–3058.

Oceanographic atlas of the Black Sea and the Sea of Azov. Eremeev, V.M. et al. (Eds.), 2009. Kyiv, Derzhgydrografia, 356 pp.

O'Donnell, J., 1990. The formation and fate of a river plume: A numerical model. J. Phys. Oceanogr. 20, 551–569.

Oguz T., Besiktepe S., Bastürk Ö., et al., 1993. CoMSBlack'92 a physical and chemical intercalibration workshop (Erdemli, 15-29 January 1993) / Workshop report. UNESCO, Intergovernmental Oceanographic Commission.

Oguz, T., Malanotte-Rizzoli, P., Aubrey, D., 1995. Wind and thermohaline circulation of the Black Sea driven by yearly mean climatological forcing. J. Geophys. Res. 100C, 6845-6863.

Schlitzer, R., 2020. Ocean Data View. https//odw.awi.de

Whitney, M.M., and Garvine, R.W., 2005. Wind influence on a coastal buoyant outflow. J. Geophys. Res. 110, C03014. https://doi.org/10.1029/2003JC002261.

Wilkin, J.L., Chapman, D.C., 1987. Scattering of continental shelf waves at a discontinuity of shelf width. J. Phys. Oceanogr. 17, 713-724.

Wu, T., Wu, H., 2018. Tidal mixing sustains a bottom-trapped river plume and buoyant coastal current on an energetic continental shelf. J. Geophys. Res. Oceans, 123, 8026–8051. https://doi.org/10.1029/2018JC014105

Yankovsky, A.E., 2000. The cyclonic turning and propagation of buoyant coastal discharge along the shelf. J Marine Res. 58, 585-607.

Yankovsky, A.E., Chapman, D.C., 1995. Generation of mesoscale flows over the shelf and slope by shelf wave scattering in the presence of a stable, sheared mean current. J. Geophys. Res. 100, 6725-6742.

Yankovsky, A.E., Chapman, D.C., 1997. A simple theory for the fate of buoyant coastal discharges. J. Phys. Oceanogr. 27, 1386–1401.

Yankovsky, E., Yankovsky, A., 2024. The cross-shelf regime of a wind-driven supercritical river plume. J. Phys. Oceanogr. 54, 537-556. DOI: 10.1175/JPO-D-23-0012.1

Figure captions

Figure 1. The northwestern Black Sea. Triangles and asterisks are hydrometeorological and streamflow gauge stations, respectively: 1 – Ochakiv, 2 – Yuzhniy, 3 – Odesa, 4 – Kakhovka, 5 – Alexandrovka; TS = Tendra Spit.

Figure 2. Surface salinity [psu] sampled in (a) 1992 and (b) 1994. Black dots are hydrographic stations.

Figure 3. Vertical transects of (a) salinity and (c) temperature in 1992, with station numbers shown at the top of panel (a). The transect is denoted with red lines on the map in panel (b), where green shading represents water depth exceeding 10 m.

Figure 4. Same as in Figure 3, but for the 1994 survey.

Figure 5. Time series of the combined Dnipro – P. Buh freshwater discharge (solid line), zonal (dotted line) and meridional (dashed line) wind components measured at Ochakiv station for (a) 1992 survey, and (b) 1994 survey. Survey time period is shown with a double arrow symbol.

Figure 6. Nearshore salinity records at stations Ochakiv and Yuzhniy in (a) May 1992, and (b) May 1994.

Figure 7. Estimate of a coastal sea level perturbation associated with the geostrophic buoyancy current (heavy blue line) and the observed sea level standard deviations at Ochakiv (red), Yuzhniy (black), and Odesa (green) shown over the freshwater discharge range for a corresponding year.

Figure 8. Aqua MODIS enhanced natural color images of NWS obtained on (a) 27 May, (b) 1 June, (c) 8 June, (d) 10 June, (e) 13 June, 2003.

Figure 9. Time series (a) as in Figure 5, and (b) as in Figure 6 but for three hydrometeorological stations; May-June 2003. Black arrows represent times of satellite images.

Figure 10. Same as in Figure 8, but for (a) 30 May, and (b) 31 May 2005.

Figure 11. Same as in Figure 9, but for May 2005.